The Impact of Autonomous Inflow Control Valve on Improved Oil Recovery in a Thin-Oil-Rim Reservoir

Soheila Taghavi[1,2*], Haavard Aakre[2], Seyed Amin Tahami[1], and Britt M. E. Moldestad[1]

[1]University of South-Eastern Norway
[2]InflowControl AS

Summary

Oil production from thin-oil-rim fields can be challenging as such fields are prone to gas coning. Excessive gas production from these fields results in poor production and recovery. Hence, these resources require advanced recovery methods to improve the oil recovery. One of the recovery methods that is widely used today is advanced inflow control technology such as autonomous inflow control valve (AICV). AICV restricts the inflow of gas in the zones where breakthrough occurs and may consequently improve the recovery from thin-oil-rim fields. This paper presents a performance analysis of AICVs, passive inflow control devices (ICDs), and sand screens based on the results from experiments and simulations. Single- and multiphase-flow experiments are performed with light oil, gas, and water at typical Troll field reservoir conditions (RCs). The obtained data from the experiments are the differential pressure across the device vs. the volume flow rate for the different phases. The results from the experiments confirm the significantly better ability of the AICV to restrict the production of gas, especially at higher gas volume fractions (GVFs). Near-well oil production from a thin-oil-rim field considering sand screens, AICV, and ICD completion is modeled. In this study, the simulation model is developed using the CMG simulator/STARS module. Completion of the well with AICVs reduces the cumulative gas production by 22.5% and 26.7% compared with ICDs and sand screens, respectively. The results also show that AICVs increase the cumulative oil production by 48.7% compared with using ICDs and sand screens. The simulation results confirm that the well completed with AICVs produces at a beneficial gas/oil ratio (GOR) for a longer time compared with the cases with ICDs and sand screens. The novelty of this work is the multiphase experiments of a new AICV and the implementation of the data in the simulator. A workflow for the simulation of AICV/ICD is proposed. The simulated results, which are based on the proposed workflow, agree with the experimental AICV performance results. As it is demonstrated in this work, deploying AICV in the most challenging light oil reservoirs with high GOR can be beneficial with respect to increased production and recovery.

Introduction

In a typical thin-oil-rim field, a thin oil layer lies between a gas cap and an underlying aquifer. Oil may be produced from such fields by drilling long horizontal wells or long multilateral horizontal wells. Oil production from such fields will, over time, cause gas coning in some locations along the well. Generally, thin-oil-rim reservoirs are prone to gas coning (Hasan et al. 2010). Excessive gas production from a gas cap will result in upward movement and smearing of the tiny oil column (Langaas et al. 2020). Therefore, oil production from a thin-oil-rim field can be challenging. The Troll field in the northern part of the North Sea is characterized as a thin-oil-rim reservoir.

The major challenge in oil production is to increase the recovery factor. The Norwegian Continental Shelf is one of the leading regions in oil recovery, but still about half of the oil on average is remaining in the reservoir after shutting down the wells. These resources require the implementation of other methods beyond the methods in the plan for development and operation to improve the oil recovery.

Well placement, well type, well path, and completion methods are among the important factors that must be evaluated to achieve enhanced well performance and improved recovery (Chan et al. 2014; Carpenter 2015). Several measures regarding the production of the thin remaining oil columns at the Troll oil field have been in focus in recent years. These measures include, but are not limited to, developing and implementing new technologies for cost-effective drilling, more accurate well placement, and technology for constraining water and gas production from the oil wells (The Norwegian Petroleum Directorate 2021). Constraining the water and gas production and consequently increasing the oil production can be achieved by deploying passive and autonomous inflow control devices (ICDs and AICDs). Both data from experiments in laboratories and the application of AICDs in reservoirs with high GOR have demonstrated that utilizing AICDs is a robust method in restriction of gas production and improving oil recovery (Konopczynski et al. 2022; Langaas et al. 2019; Tusimin et al. 2020). The production results from the well completed with rate-controlled production (RCP) valves at Troll show approximately 20% higher cumulative oil production compared with ICDs (Halvorsen et al. 2012). In addition, the GOR in wells completed with ICDs is three times the GOR in wells completed with RCPs (Halvorsen et al. 2012). Also, analysis of the output from oil wells at Troll demonstrates a clear improvement in the production rate after AICD installation (The Norwegian Petroleum Directorate 2019). The AICD completion in a superthin-oil-rim reservoir in the East and West Belumut fields in Malaysia demonstrates 50% more oil production compared with the offset ICD wells (Mohd Ismail et al. 2018).

There is an incentive to keep the production of oil at a high liquid rate before gas from the gas cap breaks through into the well. Also, it is important to keep a high oil production rate after the gas breakthrough occurs. This can be achieved by using AICVs. AICD is an autonomous inflow control device covering a wide range of devices, while AICV is one type of AICD. The effective flow area of the AICV is changing because of its dynamic and autonomous behavior, while a passive ICD has a constant flow area. AICV delays the onset of breakthrough and restricts the gas production locally when the gas breaks through into the well as it is shown in **Fig. 1** (Aakre et al. 2014)**.** The figure shows a horizontal well completed with AICVs in a heterogeneous reservoir. The pressure drops at different reservoir locations are plotted. Gas and water breakthrough occurs in high-permeability zones in heterogeneous reservoirs. In high-permeability zones, the

*Corresponding author; email: soheila.taghavi@inflowcontrol.no

Original SPE manuscript received for review 30 May 2023. Revised manuscript received for review 13 November 2023. Paper (SPE 218393) peer approved 26 November 2023.

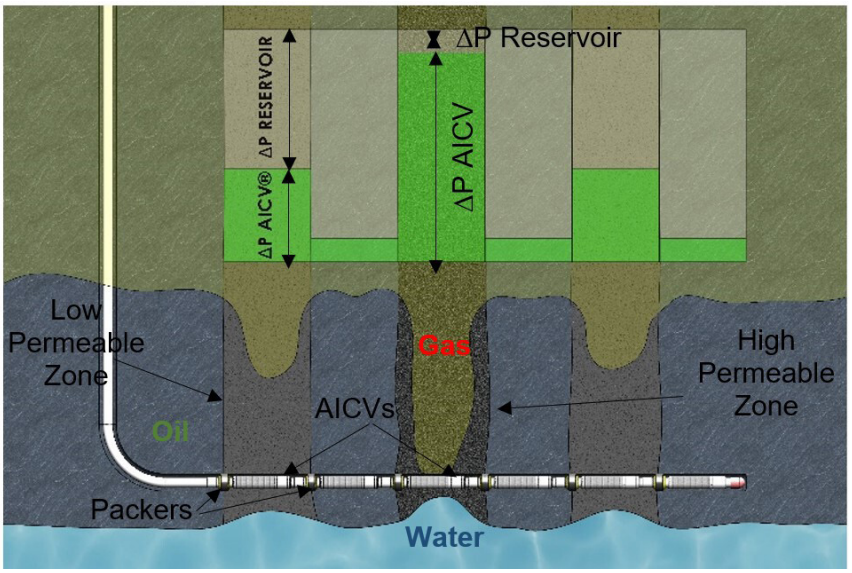

Fig. 1—High pressure drop across AICV in high-permeability zones with gas and water breakthrough (Aakre et al. 2014).

low resistance in the reservoir gives a high flow rate of fluids resulting in a higher pressure drop through the AICV, indicating that the AICV is choking. However, in low-permeability zones, the pressure drop in the reservoir is higher and as the total pressure drop from the reservoir to the well is constant, the pressure drop over the AICV is lower. The reduction of gas production from the breakthrough zones allows to keep a low bottomhole pressure. This keeps a higher sandface drawdown in the zones with oil and thus keeps the oil production from these zones. This results in maximizing the oil production and recovery. The increased oil production and reduced water and gas production obtained by using AICV are demonstrated in several field installations worldwide, and the results are presented in several studies (Alakberi et al. 2023; Buwauqi et al. 2021; Kearns et al. 2022).

According to Halvorsen et al. (2012), the RCP valves have increased the cumulative oil production by 20%. The single- and multiphase behaviors of the new AICV presented in this work are evaluated to find if the AICV can additionally increase the cumulative oil production. This new AICV has a better performance in multiphase flow compared with previous versions of AICVs.

The objective of this paper is to evaluate the performance of the new AICV in a thin-oil-rim reservoir and its impact on reservoir recovery. This is achieved by performing experiments and simulations. The experimental study includes one-phase and multiphase flow tests for orifice ICD and AICV using water, gas, and oil as the reservoir fluids at realistic RCs. Simulations are performed using a commercial simulator. The impact of improved AICV performance on the reservoir recovery is evaluated, and the results are validated against the experimental data.

AICV Technology and Design for Light Oil

The technology developed by InflowControl AS (the AICV; see **Fig. 2a**) restricts the production of unwanted fluids such as water, gas, and steam significantly. By balancing the reservoir drawdown, AICV delays the onset of water and/or gas breakthrough, and in case of breakthrough, it will restrict the production of these unwanted fluids significantly. **Fig. 2b** shows an AICV mounted in a base pipe with sand screen. Annular swellable packers must be in place to provide robust zonal and annulus isolation. Perfect sectioning of the annulus will guarantee the functionality of AICV in long horizontal wells.

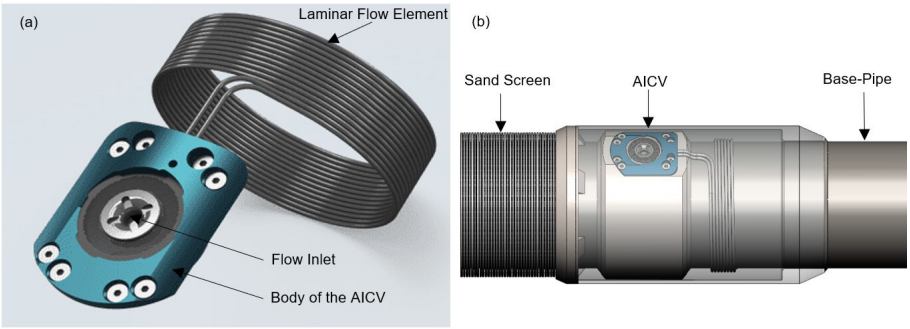

Fig. 2—AICV design for light oil (a) and AICV mounted in a base pipe with sand screen (b).

The AICV distinguishes between the reservoir fluids and reacts accordingly. The functionality is based on the viscosity and density of the reservoir fluids. The valve keeps open for viscous fluids like light oil and closes for lower viscous fluids such as water and gas. Light oil is defined as oil with a density of less than 875.7 kg/m^3 (API gravity greater than 30.1 °API) (Canadian Legal Information Institute 1996). In this paper, the viscosity of the oil is 2.1 cp and the density is 870 kg/m^3 at RCs, which is considered light oil.

The functionality of the AICV is controlled by a pilot flow parallel to the main flow, as it is illustrated in **Fig. 3.** The main body, inlet, and piston are the elements of the main flow path. The pilot flow consists of a pipe segment and a thin-plate orifice that are connected in series. The pipe segment serves as a laminar flow element (LFE) and the pressure drop through it is proportional to the fluid viscosity and the velocity. Eq. 1 describes the pressure drop through the LFE:

$$\Delta P = f \times \frac{L\rho v^2}{2D} = \frac{64}{\mathrm{Re}} \times \frac{L\rho v^2}{2D} = \frac{32\mu v L}{D^2}, \tag{1}$$

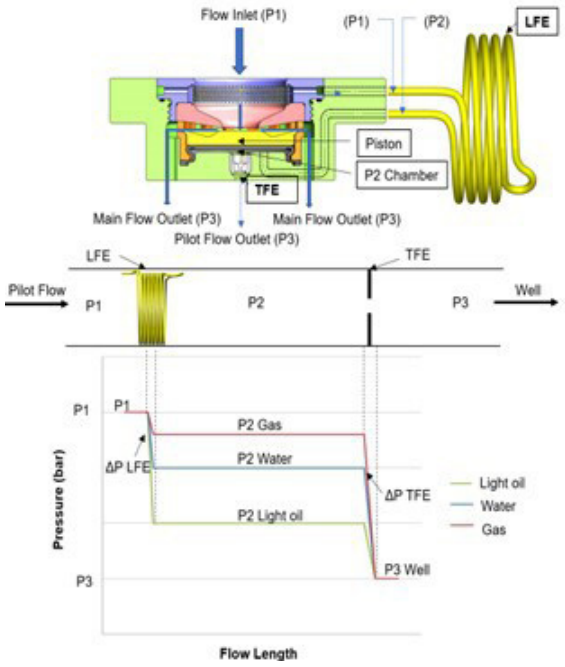

Fig. 3—Pressure drop of reservoir fluids through the AICV.

where ΔP is the pressure drop, f is the friction factor (64/Re), Re is Reynolds number, ρ is the fluid density, μ is the fluid viscosity, v is the fluid velocity, and L and D are the length and diameter of the LFE, respectively. A thin-plate orifice serves as a turbulent flow element (TFE) and the pressure drop through it is given by Eq. 2:

$$\Delta P = \frac{1}{2C_d^2}.\rho v^2, \tag{2}$$

in which C_d is the discharge coefficient that depends on the orifice design (Konopczynski et al. 2022). The discharge coefficient is a dimensionless number that is used to characterize the pressure loss behavior of an orifice or a nozzle and is defined as $C_d = A/A_{VC}$ (Moradi and Moldestad 2021). A is the cross-sectional area of the orifice hole and A_{VC} is the area in vena contracta. Vena contracta is the minimum jet area that appears just downstream of the orifice, where the fluid velocity is at its maximum.

As it is illustrated in **Fig. 3**, the reservoir fluid at reservoir pressure P1 enters the valve inlet, and a minor portion of the fluid is guided through the pilot flow elements, while the main flow passes through the small opening between the inlet seat and the piston. By passing through the LFE, the pressure of the fluid is reduced to P2 at a chamber called the P2 chamber. The fluid properties and the flow rate through the pilot flow determine the P2 pressure. The pilot flow is further led through the turbulent flow element in which the second pressure drop to the well pressure, P3, occurs. The P2 pressure in the P2 chamber controls the valve functionality. Different P2 pressures act on the piston based on the different fluids passing through the LFE. For higher viscosity fluids like oil, the pressure drop through the LFE is high, resulting in a lower P2 (see the lower plot in **Fig. 3**). Because the P2 pressure is low for oil, the generated force under the piston, which acts upward, is low as well. This will keep the piston in an open position, producing oil to the well through both the main flow and the pilot flow path. For lower viscosity fluids, such as gas and water, the pressure drop through the LFE is low, resulting in a higher P2 (see the lower plot in **Fig. 3**). Because the P2 pressure is high for gas and water, the generated force under the piston, which acts upward, is high as well. This will actuate the piston and the valve will close. The closed valve produces gas and water to the well only through the pilot flow path.

The LFE, the turbulent flow element, the inlet, and the piston design are adapted to the conditions, including the reservoir fluid properties and the requirements in the relevant field. The force balance around the piston is described in detail in earlier scientific works (Aakre et al. 2013, 2014).

Single- and Multiphase Flow Loops and Test Conditions

Fig. 4 shows the photo and the piping and instrumentation diagram of the flow loop test rig. The test facility is designed for single- and multiphase oil, water, and gas tests. Performance curves from single-phase tests with oil, gas, and water are obtained from the test rig. Performance curves describe the differential pressure of the AICV and ICD as a function of volumetric flow rate of the fluid. Also, the closure function of the AICV is obtained from the multiphase tests with oil and gas and/or oil and water.

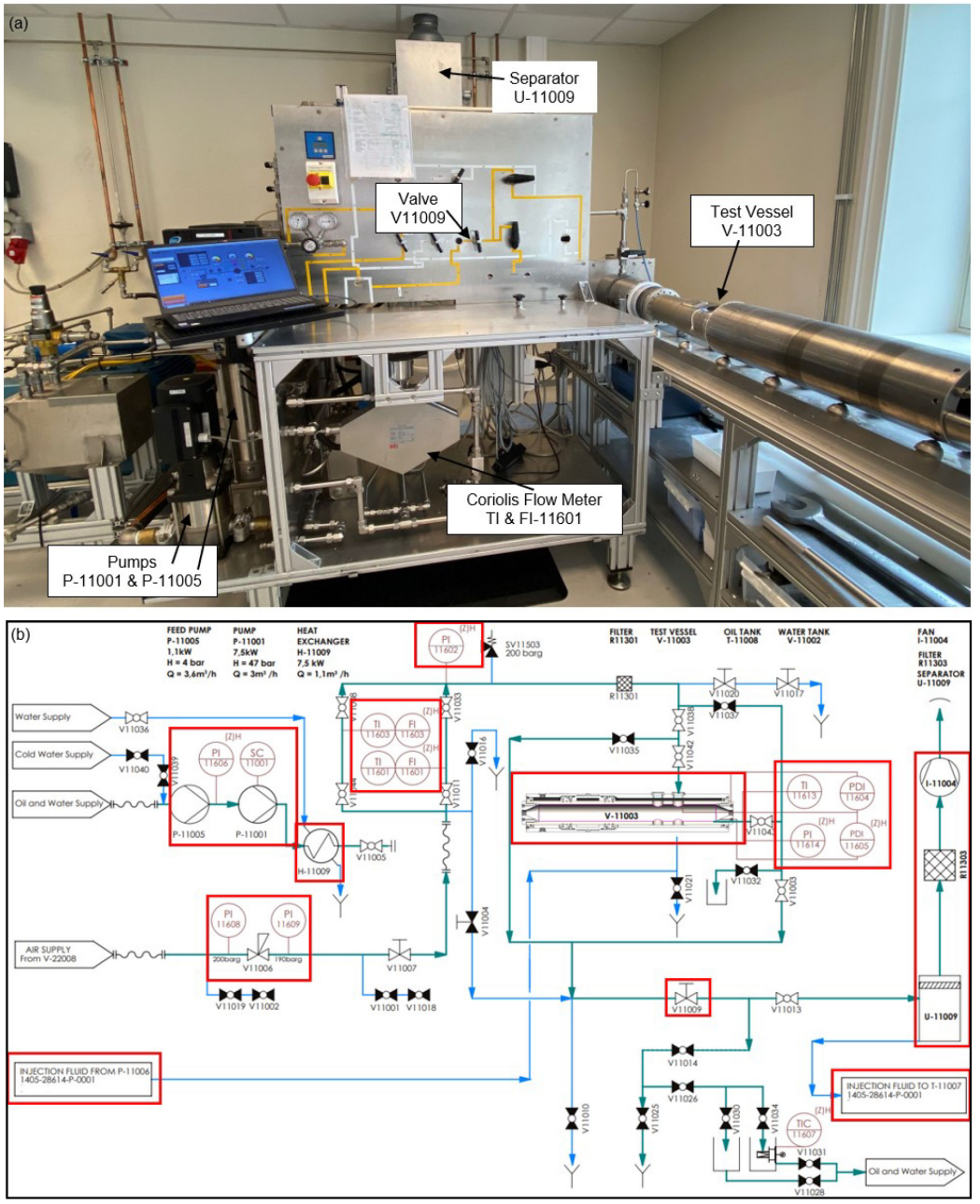

Fig. 4—Photo (a) and piping and instrumentation diagram (b) of the flow loop test rig showing the key elements and measuring instruments marked with red rectangles.

Two pumps, P-11005 and P-11001 in series, are used to increase the liquid pressure up to 50 bar from the oil and water supply. Compressed air at room temperature is regulated by V-11006 to the desired pressure for each case, up to a maximum of 200 bar. An AICV or ICD is installed in the test vessel, V-11003. Flow rates, density, and temperature are measured by the Coriolis flowmeters, TI & FI-11601 and TI & FI-11603, which are located close to the test vessel inlet. Pressure transmitter PI-11602 measures the inlet pressure, whereas the differential pressure transmitters, PDI-11604 and PDI-11605, measure the total differential pressure over the test vessel. Also, TI-11613 and PI-11614 measure the temperature and pressure of the outlet fluid, respectively. Valve V11009 is used to control and regulate the fluid flow rate. The fluids are circulated back to the oil and water supply and air exits to the atmosphere after passing through the separator, U-11009, and filter, R11303. The heat exchanger, H-11009, is used to regulate the temperature of the circulated fluid to the desired temperature. To study the multiphase behavior of the AICV or ICD, the test vessel is already filled with gas, and the desired amount of oil is injected by Pump P-11006 from a separate test unit that is connected to the single-phase test rig. After passing through the inflow device, oil and gas are separated in the separator where oil is circulated back to the oil supply tank, T-11007, in the injection rig and gas exits to the atmosphere after passing through the filter. All the key elements and measuring instruments of the test rig are marked with red rectangles in **Fig. 4b**.

The controlled and measured key variables for the test program were flow rates, differential pressure across the AICV or ICD, system conditions (pressure and temperature), and fluid properties, such as viscosity and density. The test matrix and system condition applied in the experiments are given in **Table 1.** These conditions represent the Troll field conditions. The tests are performed at different temperatures and pressures to obtain the viscosity and density of the fluids in the reservoir. The differential pressure across the AICV or ICD is

varied gradually between 1 bar and 20 bar. The flow rate and differential pressure are continuously measured as the differential pressure is gradually varied from 1 bar to 20 bar. The air density is equivalent to the hydrocarbon gas density at theRCs.

Description	Fluid Type	Density (kg/m^3)	Viscosity (cp)	Pressure (bar)	Temperature (˚C)	Differential Pressure (bar)
Single-phase test	Pressurized air	92	0.02	78	21	1–20
	Water	980	0.41	50	68	1–20
	Oil	870	2.1	50	21	1–20
Multiphase test	Oil and gas	–	–	78	21	10, 15, 20

Table 1—Test conditions.

Development of the Reservoir and Well Model in a Commercial Simulator

In this study, CMG STARS is used to model the performance of ICD and AICV in a light oil reservoir. The developed model investigates the performance of ICD and AICV and their effect on increased oil recovery. CMG STARS is a reservoir simulator capable of handling multiple phases and components. Besides, when modeling a well with CMG STARS, two options are available, which are the source/sink model and the advanced FlexWell (FW) model. The source/sink model is suitable for specific scenarios, such as short horizontal wells, uniform wellbore-reservoir communication, low flow rates, or large pipe diameters. FW is an advanced wellbore model that considers complex well completions, utilizing governing equations for mass, energy, momentum balance, and pipe flow with spatial discretization (Mohd Ismail et al. 2021). FW modeling incorporates a two-way interaction between the wellbore and reservoir simulator, capturing dynamic interactions. This modeling process involves solving the wellbore and reservoir models alternately at each time step, with the reservoir slightly trailing behind by one iteration. As a result, to enhance the precision of the well modeling calculations, CMG STARS is used for reservoir modeling, and the FW option is chosen for modeling the wells equipped with ICDs and AICVs.

Reservoir Model. The reservoir properties at the Troll oil field are used to develop a thin-oil-rim reservoir model in the simulator. The Troll oil field is located in the North Sea, 80 km from the west coast of Norway. The oil production from the Troll West oil and gas province started in 1995. The thin oil layer was originally between 22 m and 26 m at the Troll West oil province, located at a depth of 1360 m (Mjaavatten et al. 2006). The thin oil layer lies between a large gas cap and a strong aquifer. The oil column is now reduced to only 1–5 m in thickness (The Norwegian Petroleum Directorate 2021). However, a significant volume of residual oil is encountered directly below the oil column (The Norwegian Petroleum Directorate 2021). The newly drilled long horizontal multilateral wells at the Troll oil field have a reservoir length of more than 3500 m. These wells are positioned close to the oil-water contact to avoid early gas breakthrough. The Troll reservoir mostly consists of high-permeability homogeneous sandstones with permeability ranging from 1 darcy to more than 20 darcies. In addition, the porosity ranges from 30% to 35% (Halvorsen et al. 2012).

Reservoir Fluid and Rock Properties. The temperature of the reservoir near the well is 68°C and the pressure at initial conditions is 12 500 kPa, and it is assumed to be constant. The most important properties of the fluid used for the simulation are presented in **Table 2.** The light oil viscosity as a function of pressure at reservoir temperature is shown in **Fig. 5.**

Parameter	Value at 68°C	Unit
Viscosity	2.1	cp
Density	870	kg/m^3
GOR	42	std m^3/std m^3
Bubblepoint pressure	12 500	kPa

Table 2—Oil properties.

The reservoir near the well has a total oil column of 7 m, starting from a depth of 2092 m. The effective porosity of sandstone near the well is 30%. Generally, it is challenging to obtain information about relative permeability for different fields. Veskimägi (2013) presented relative permeability data provided by the Equinor Troll department in his work. The study uses the standard type of unnormalized LET family of correlations (Lomeland and Orec 2018). The calculated LET relative permeabilities were a good match for the historic well production. The relative permeability curves for oil, water, and gas at the Troll reservoir are presented in **Fig. 6.**

The permeability of the heterogeneous reservoir in both *x*- and *y*-directions varies from 42 md in the low-permeability zones to 7,282 md in the relatively high-permeability zones. The vertical permeability is specified in each block of the reservoir, and it varies from 20 md to 5,058 md for the low-permeability and the relatively high-permeability zones, respectively. These values are the average permeabilities in each production zone (Veskimägi 2013). This is to illustrate a heterogeneous reservoir. The horizontal and vertical permeability profiles of the heterogeneous reservoir are illustrated in **Fig. 7.** The capillary forces are not included in this study. The objective of this work is to evaluate the AICV performance and compare it with ICD and screens under the same conditions. It is expected that the inclusion of capillary forces will not affect the outcome of this work.

Dimensions of the Reservoir Drainage Area and Grids. In this work, for simplicity, a rectangular drainage area is considered for developing the oil production model. The length of the drainage area is 4500 m, the length of the horizontal well is 3500 m, and the width of the drainage area is 201 m. The thin oil column is placed between a gas cap starting at the depth of 2026 m and an underlying aquifer. It is assumed that the well is located at a depth of 2096 m in the thin oil column and 4 m below the gas cap. The size of the blocks varies along the *y*- and *z*-directions, while a uniform mesh along the *x*-direction is defined. Based on the mesh-sensitivity analysis performed by Timsina et al. (2017), finer mesh along the *x*-direction will have an insignificant impact on the overall flow rate. The optimal required number of grids in (*x*, *y*, *z*) coordinates and their size for discretizing the reservoir near the well have been determined and are presented in **Table 3.**

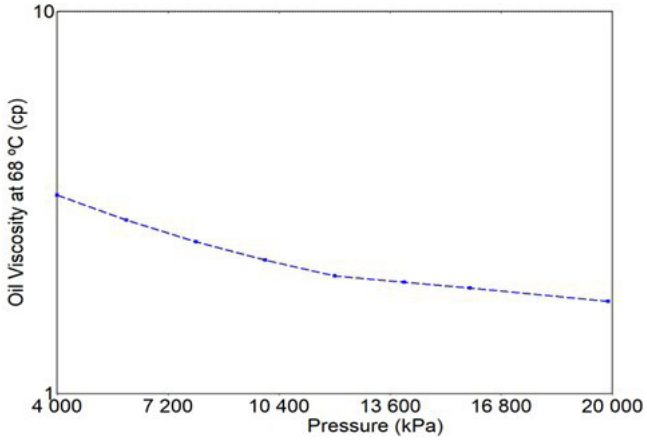

Fig. 5—Oil viscosity as a function of pressure.

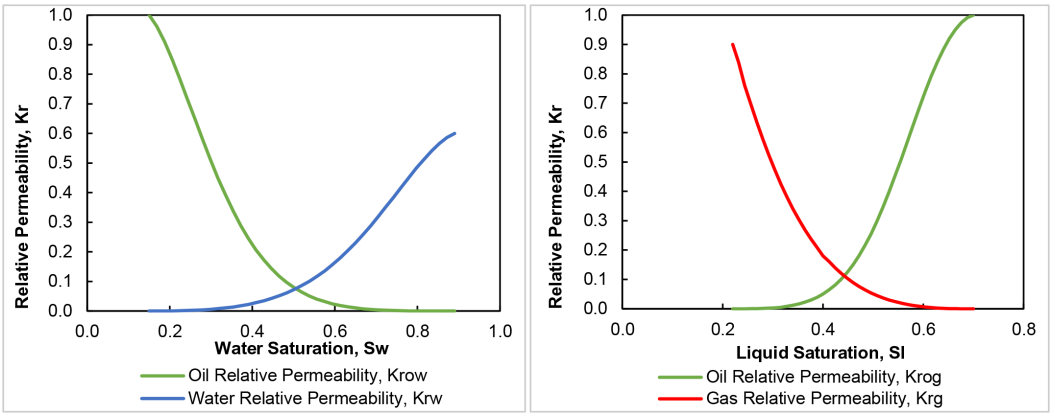

Fig. 6—LET relative permeability curves for the Troll reservoir (Veskimägi 2013).

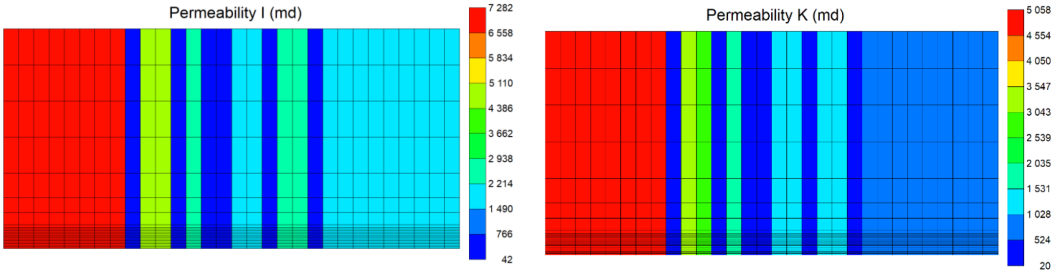

Fig. 7—Permeability profile of (left) horizontal permeability and (right) vertical permeability.

Direction	Length (m)	Number of Blocks	Block Size (m)
x	4500	30	150 (constant)
y	201	15	30, 24, 20, 12, 8, 4, 2, 1, 2, 4, 8,12, 20, 24, 30
z	73	22	12, 12, 12, 12, 8, 5, 4, 1, 0.5, 0.5, 0.5, 0.5, 0.5, 0.5, 0.5, 0.5, 0.5, 0.5, 0.5, 0.5, 0.5, 0.5, 0.5, 0.5

Table 3—Drainage area grid dimension.

Fig. 8 shows the grid resolution in IK-2D and JK-2D cross-sectional views and the position of the well. The scales are *Z*/*X*: 31:1 and *Z*/*Y*: 1.4:1.

Reservoir Initialization. The model is initialized without engaging the calculation of gravity equilibrium. The temperature of the reservoir is set at 68°C, while the initial pressure is considered constant (equal to 12 500 kPa) during the initialization. In Layers 1–8 in the *z*-direction, all the blocks are fully saturated with gas, whereas Layers 9–22 are initially set with 85% oil saturation and 15% water saturation.

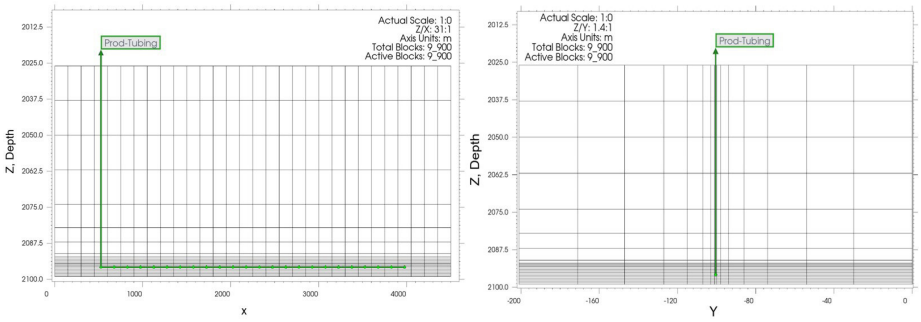

Fig. 8—Grid resolution in (left) IK-2D and (right) JK-2D cross-sectional views and the well position.

Wellbore Model. The model is run for 5 years to investigate the oil production. The minimum and maximum timesteps are set to 0.00001 days and 0.25 days, respectively. The well model consists of two pipes that represent the wellbore and the production tubing. The wellbore is a pipe with a length and inner diameter of 3500 m and 0.2159 m (8.5 in.), and the production tubing is a pipe with a length and inner diameter of 3500 m and 0.1397 m (5.5 in.).

To mechanistically model the simulation period, FWs were defined in the simulator. The FWs are annulus and tubing, both of the producer type. Three different completion scenarios are modeled and compared. Sand screens only, well completed with ICDs, and well completed with AICVs are simulated. By considering the target oil production rate and using the single-phase experimental data for oil shown in **Fig. 9,** the required number of AICVs and ICDs is determined. The oil flow rate through each AICV and ICD at around 10–15 bar drawdown is measured to be approximately 0.4 m^3/h. It is assumed that 2500 m^3/d oil is produced from 24 zones along the entire horizontal section. In each zone, 12 AICVs or 12 ICDs are used. To avoid the annular flow of the reservoir fluids, each production zone is isolated by packers installed in the annulus.

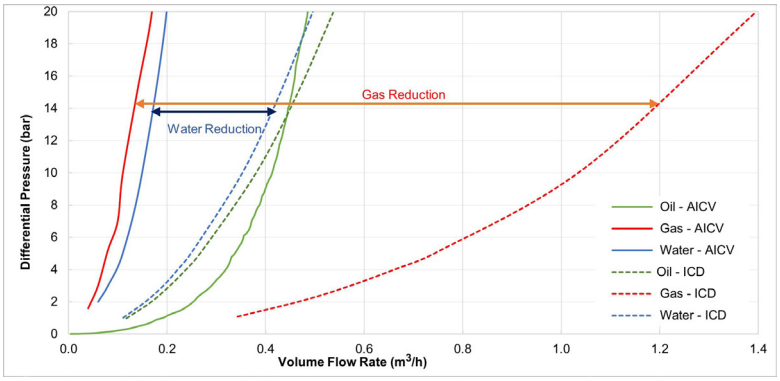

Fig. 9—Experimental performance curves for oil (2.1 cp), gas (0.02 cp), and water (0.41 cp) for ICD and AICV.

The production constraints are maximum surface liquid rate of 2500 m^3/d, minimum bottomhole pressure of 11 000 kPa, and GOR to stay below 600 std m^3/std m^3, with a cutback rate of 0.85 for the 5 years of production. The specifications of FWs and constraints for the production tubing are given in **Table 4.**

		Constraints			
Well	Well Size, Wall ID	Parameter	Limit/Mode	value	Action
Producer FW, annulus	0.2159 m (8.5 in.)	—	—	—	—
Producer FW, tubing	0.1397 m (5.5 in.)	Surface liquid rate	MAX	2500 m^3/d	Continue (CONT)
		Bottomhole pressure	MIN	11 000 kPa	Continue (CONT)
		GOR	STG	Upper limit	Continue (CONT)
				Cutback rate	

Table 4—Well configurations and constraints.

AICVs and ICDs are placed in the production tubing every 12.5 m, and their effects on oil production and gas reduction are investigated. In the simulations, AICV/ICD tables are developed and used to implement their behavior using the characteristics of the AICV/ICD and the reservoir fluid mixtures. The flow control device (FCD) table allows for characterization of an FCD through tabulated data. In this work, the AICV and ICD tables are based on experimental data shown in **Figs. 10 and 11.** The dependent variables to generate the FCD tables are the gas mass fraction and volume flow rate. A workflow for developing the AICV/ICD tables in the simulator is proposed in Appendix A.

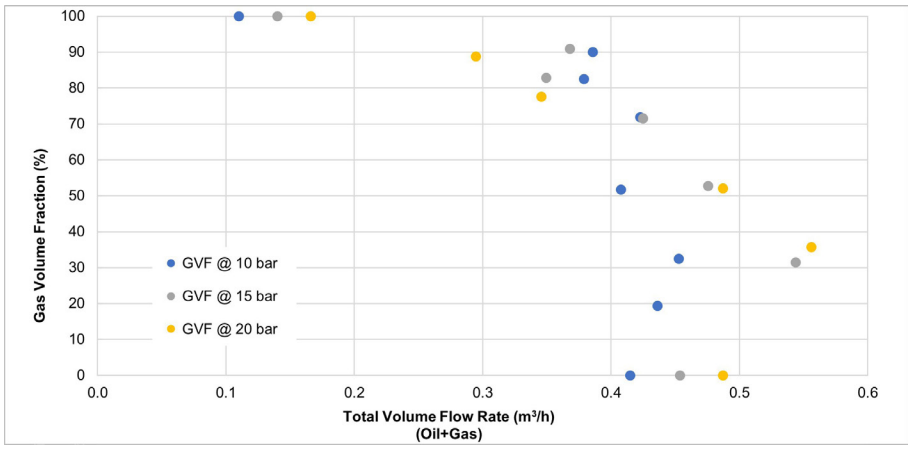

Fig. 10—Experimental GVF as a function of two-phase oil/gas volume flow of oil (2.1 cp) and gas at 10-bar, 15-bar, and 20-bar differential pressures across the AICV.

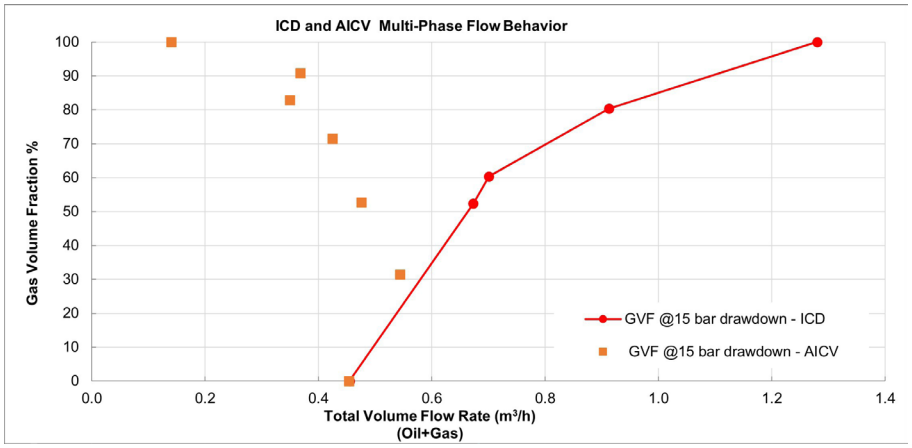

Fig. 11—Experimental multiphase flow behavior for ICD and AICV.

Simulation Cases. In this paper, the impact of AICV on improved oil recovery in a thin-oil-rim reservoir is evaluated. To achieve this purpose, in addition to the main study case with AICV completion, the simulations are conducted for similar cases with ICD completion and one case that represents sand screens only. AICV and ICD used in the experimental tests have the same strength. The strength of AICV or ICD is defined as the pressure drop over the valve when the oil flow rate is equal to 1 m^3/h. The completion scenarios are summarized in **Table 5.**

Completion Scenario	Number in Each 150-m Zone	Total Number	Diameter
Sand screens	12	288	8-mm ICD (as an approximation for sand screens only)
ICD	12	288	2.1 mm
AICV	12	288	Same strength as ICDs

Table 5—Completion scenarios.

The simulations for all the different cases have been performed for 5 years of production using the same well constraints as listed in **Table 4**.

Results and Discussion

The experiments and simulation results are presented and discussed in the following subsections.

Experimental Single-Phase Flow Test. AICV and an orifice-type ICD with 2.1-mm diameter and discharge coefficient of 0.65 for all the phases are used for the single-phase experiments under the Troll field conditions. The single-phase experimental results have been obtained for oil, water, and pressurized air. The results shown in **Fig. 9** represent the performance curves of the AICV and ICD. The performance curves illustrate pressure drop across the devices as a function of volumetric flow rate for single-phase fluids. At a 15-bar pressure drop, the oil/water ratio for AICV is 2.60, while it is 1.08 for ICD. Also, the oil/gas ratio at the same pressure drop for AICV

is 3.20, while it is 0.36 for ICD. The corresponding values of the oil/water ratio and oil/gas ratio for the RCP valve are 1.33 and 0.55, respectively, at a 15-bar pressure drop at Troll conditions (Halvorsen et al. 2016). The approximate fluid ratio values for the ICD, the RCP valve, and the AICV are summarized in **Table 6.**

Device	Oil/Water Ratio	Oil/Gas Ratio
ICD	1.08	0.36
RCP valve	1.33	0.55
AICV	2.60	3.20

Table 6—Approximate fluid ratio values for ICD, RCP valve, and AICV.

The oil flow rates through the ICD and AICV are equal at a 15-bar pressure drop, and the differences in the flow characteristics are studied. At a 15-bar pressure drop, the gas and water flow rates through the passive ICD are approximately 7.35 and 2.4 times more compared with AICV. The results indicate that the gas and water reduction by using AICV is significant. The ICD behavior is mainly density dependent, and therefore the flow rate of oil and water differs slightly, while the AICV chokes the water considerably. This is favorable when an aquifer is present in the reservoir and water breakthrough is likely to occur.

Experimental Two-Phase Flow Test. The multiphase behavior of inflow control technologies is of significant importance in controlling the breakthrough and restriction of unwanted fluids such as gas and water. **Fig. 10** shows the two-phase oil/gas tests performed at 10-bar, 15-bar, and 20-bar differential pressures across the AICV. The GVF vs. the two-phase oil/gas volume flow rate is presented in **Fig. 10**. The results demonstrate how AICV restricts the gas flow rate as the GVF increases. If oil flashes in the reservoir toward the inflow zones, gas is released from the oil. When the local GVF is up to 30%, the AICV opens, allowing all the oil together with gas to flow through the valve. The AICV closes gradually from 30% GVF until 100% pure gas flows through the valve. At this point, the AICV is closed for gas and the only remaining flow is through the pilot flow.

Fig. 11 shows the comparison of the oil/gas experimental results for ICD and AICV at 15-bar differential pressure. The oil flow rate at 15-bar differential pressure through both ICD and AICV is 0.45 m^3/h. As the amount of gas (GVF) increases, AICV chokes the gas flow, while ICD does not restrict the gas production. When the GVF reaches 100%, the volume flow rate through the ICD is 1.27 m^3/h, which is three times more than the volume flow rate for pure oil through the ICD. The AICV restricts the gas flow significantly, specifically at higher GVF, which is what makes this technology unique compared with other inflow control technologies.

Simulated Fluid-Flow Distribution, Pressure and Oil Production Along the Well. Fig. 12 illustrates the *y-z* view of the oil-saturation contours for the least permeable zone (42 md) by considering AICV completion. As shown in the contours, gas is coning toward the production well and oil is being produced as the oil saturation is less around the well location and the adjacent cells. Therefore, it can be interpreted that, by use of AICV, the low-permeability zones also contribute to the oil production.

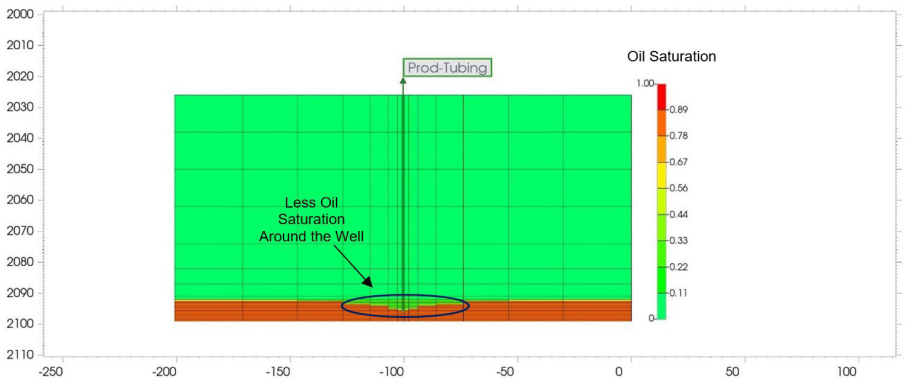

Fig. 12—Simulated oil-saturation distribution for the AICV completion in the least permeable zone.

Fig. 13 shows the tubing pressure and gas and oil flow rates along the horizontal length of the well for the cases with AICVs and sand screens at day 350 when excessive gas production occurs in the AICV case. This is to compare the best and the worst scenarios. The circles represent the flow influx from each zone, which is isolated by packers. In the high-permeability zones in the heel, which suffer from excessive gas production, the highest pressure drop occurs through the AICV, while the pressure drop with sand screens is negligible (see **Fig. 13a**). AICV chokes the gas flow rate entering the well, resulting in a higher pressure drop across the AICV in the heel while continuing to produce oil from the heel and other zones along the well (see **Figs. 13b and 13c**).

Fig. 14 illustrates the pressure in the tubing for the completion scenarios during the production period. As can be seen from the figure, AICV has the highest pressure drop ($P_{reservoir} - P_{tubing}$) over the whole production period. The higher pressure drop indicates that AICV chokes the gas flow entering the well for a longer period. This will delay the excessive gas production that will eventually take over the oil production.

Accuracy of the FCD Tables for Implementing the Behavior of the AICVs. To check if the simulated oil production agrees with the experiments, **Fig. 15** is considered. The plot to the left shows the simulated oil flow rate along the well and the tubing pressure. In production zone 1, for the case of AICVs, the pressure drop across the AICV ($P_{reservoir} - P_{tubing}$) is around 1500 kPa (15 bar) along the zone length shown by a blue ellipse. The simulated oil production for this zone is approximately 135 m^3/d. According to **Table 5**, there are 12

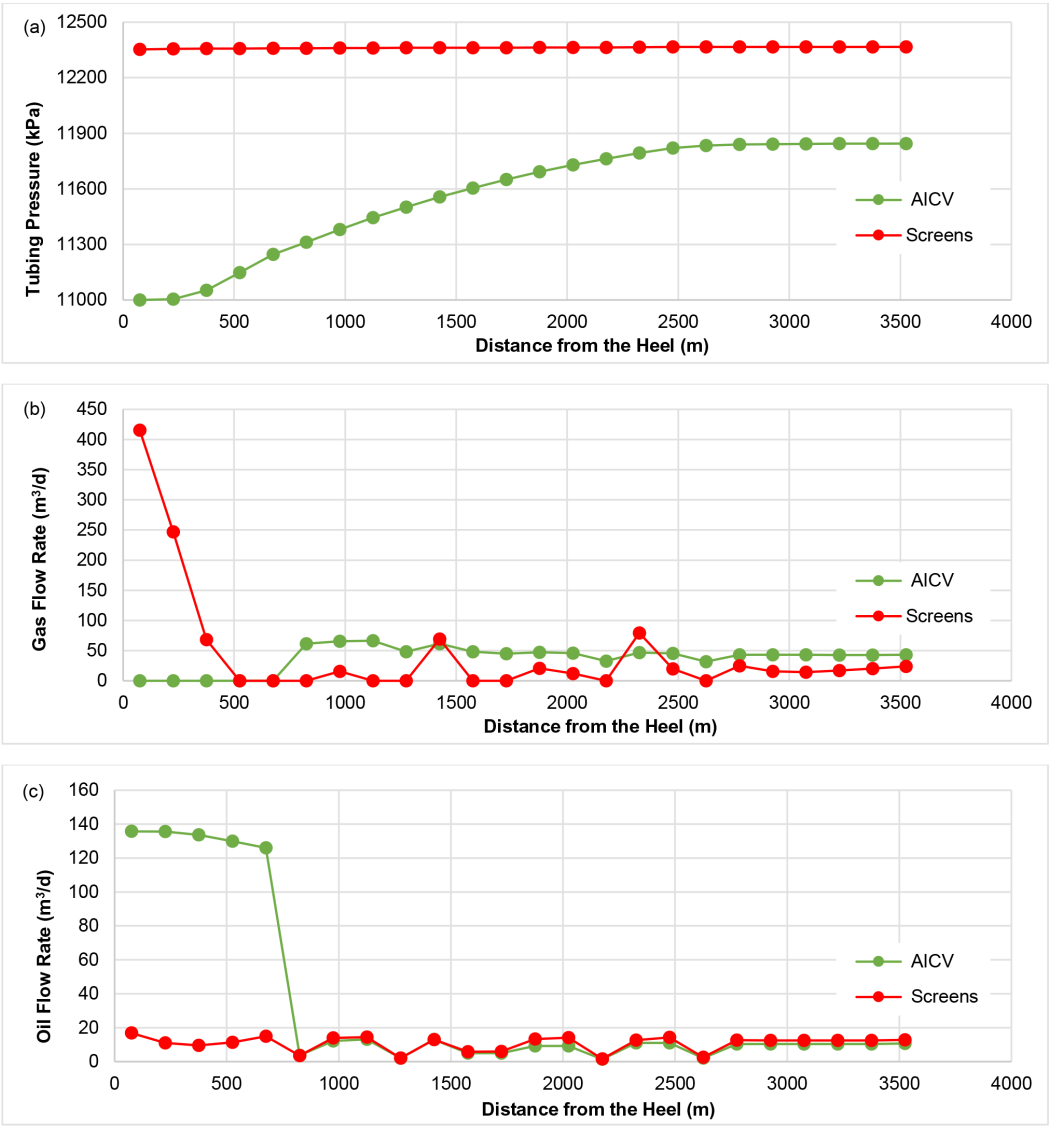

Fig. 13—Simulated tubing pressure (a), gas flow rate at RC (b), and oil flow rate at RC (c) along the well for the cases with AICV and sand screens.

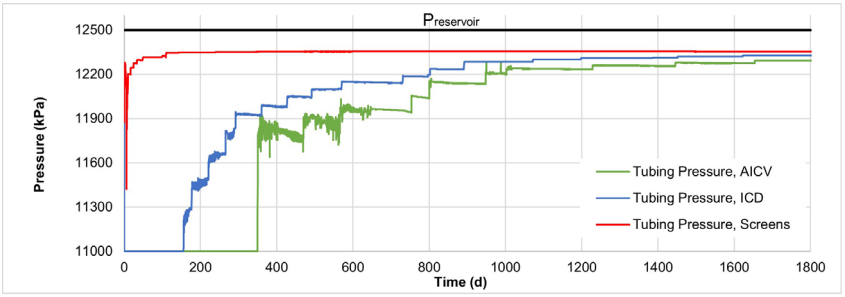

Fig. 14—Simulated pressure changes of the completion scenarios with time.

AICVs installed in this zone which implies an oil production of 11.25 m^3/d (0.46 m^3/h) per AICV. **Fig. 9** demonstrates that at around 15-bar differential pressure across the AICV, the oil flow rate is around 0.45 m^3/h. The plot to the right shows the comparison of simulated and experimental data for single-phase oil in production zone 1. The comparison indicates that the implementation of the workflow for generating the FCD table in the simulator has been successful.

Simulated GOR Development. One important parameter that must be considered for comparing the functionality of the AICVs with other types of completions is the GOR development. **Fig. 16a** illustrates the GOR development of the production well for a period

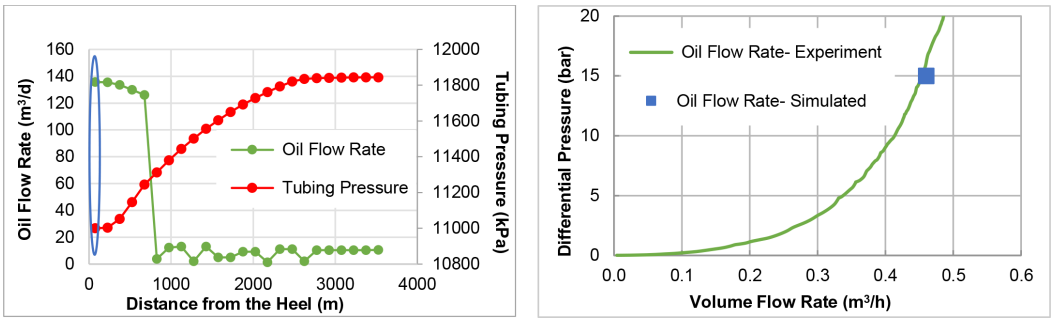

Fig. 15—Simulated oil flow rate and pressure drop across AICVs along the well (left) and oil flow rate from experiments and simulation (right).

of 1,825 days. **Fig. 16a** includes the GOR development by considering completions with both AICVs, ICDs, and sand screens. For challenging thin-oil-rim reservoirs, it is beneficial to have long-term oil production, as this limits the production from the gas cap. When the production from the gas cap is restricted, the upward movement and smearing of the oil column are limited (Langaas et al. 2020). As it can be seen from **Fig. 16a**, the early GOR level is highest with sand screens, delayed somewhat with ICDs, and even more with AICVs. The well is producing at a beneficial GOR for a longer time for the AICV case compared with the cases with ICDs and sand screens. Keeping the GOR at a relatively low level allows the production well to stay longer at a high liquid rate without needing to choke back because of high GOR.

Fig. 16b shows the GOR at standard conditions as a function of cumulative oil production at RC. This figure illustrates how the GOR varies with cumulative oil production. Usually in the wells, the total allowable gas production is limited, because the total gas processing capacity is an active constraint (Mjaavatten et al. 2006). This highlights the importance of developing new inflow control technologies that guarantee a higher maximum oil production while meeting the GOR constraint. As can be seen from **Fig. 16b**, the accumulated oil at a specific GOR (e.g., 400) for the AICV case is approximately four times more than the accumulated oil for the ICD case.

Simulated Cumulative Oil and Gas Production. Another important parameter that must be considered for comparing the functionality of the AICVs with other types of completions is the accumulated oil and gas. **Fig. 17** illustrates the cumulative oil and gas produced at RC by considering sand screens, ICD, and AICV completions along the well and by time. As it is shown in **Fig. 17a**, the cumulative oil production along the entire horizontal length of the well, at a given time, is higher for the AICV case compared with the case with screens. This implies that both the high- and low-permeability zones along the entire length of the wellbore contribute to the oil production by using AICVs. **Fig. 17b** shows that there is an insignificant difference between accumulated oil in the ICD and sand screen cases, whereas the accumulated gas drops by using ICDs compared with sand screens. However, the difference between accumulated oil in the AICV case compared with the two other cases is significant. Also, because of the choking effect of the AICVs on low-viscosity fluids like gas, the amount of accumulated gas drops significantly when the well is completed with AICVs. The values of accumulated oil and gas for the three simulated cases are presented in **Table 7.** According to **Table 7**, the cumulative oil production is 48.7% more when using AICVs

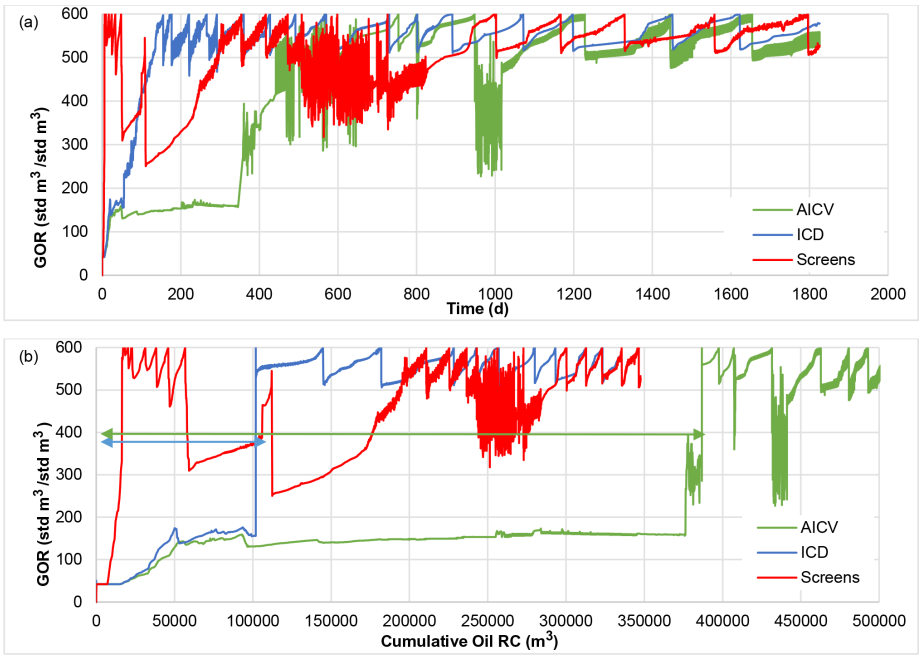

Fig. 16—Simulated GOR development for sand screens, AICVs, and ICDs simulation cases (a) and accumulated oil production vs. GOR for sand screens, ICDs, and AICVs (b).

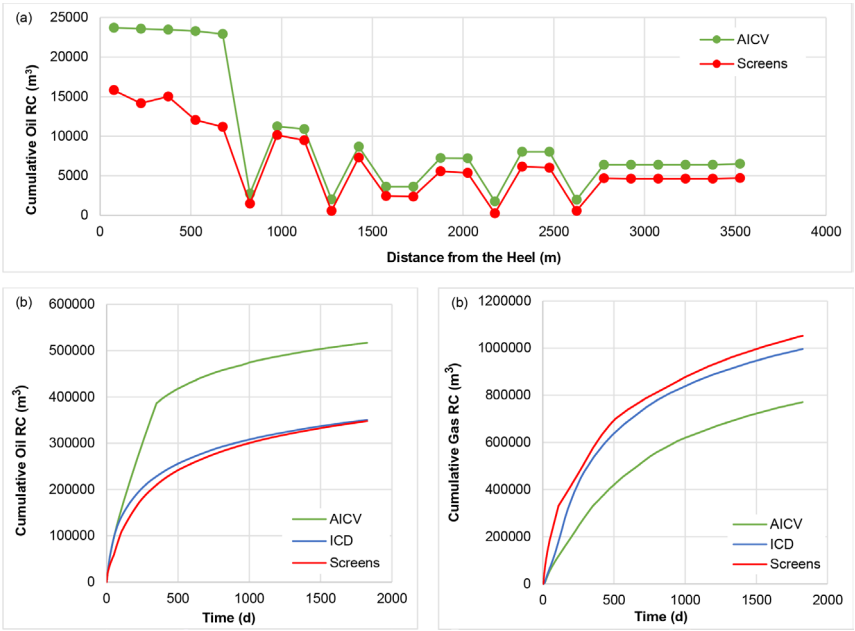

Fig. 17—Simulated accumulated oil along the well at a given time (a) and accumulated oil and gas from the well by time (b).

Completion Scenario	Accumulated Oil (m^3)	Accumulated Gas (m^3)	Relative Oil Increase from Sand Screens Case (%)	Relative Gas Reduction from Sand Screens Case (%)
Sand Screens	347 568	1 052 216	0	0
ICD	347 754	996 252	Negligible	–5.31
AICV	517 146	771 246	+48.7	–26.7

Table 7—Values of accumulated oil and gas after 1,825 days of oil production.

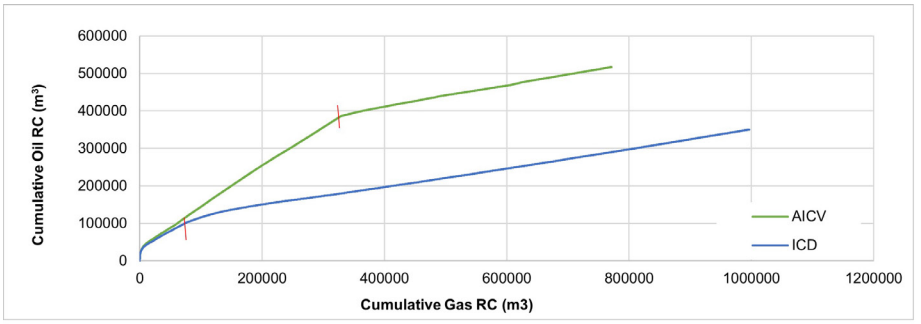

Fig. 18—Comparison of cumulative oil production as a function of cumulative gas production for well completions by ICDs and AICVs.

compared with using ICDs and sand screens. Owing to the better performance of AICV in both single- and multiphase flow regions, the amount of accumulated gas after 1,825 days of production is reduced by 22.5% and 26.7% relative to the ICD and sand screen cases, respectively. When the gas enters the well, AICV starts to choke the gas production gradually. Indeed, AICV chokes the gas production consistently as the gas mass fraction increases. This behavior, which is based on the experimental data, was implemented in the FCD control tables.

The flow influx along the horizontal well can be evened out by using AICVs. **Fig. 18** illustrates that the excessive gas production occurs much later for the case with AICVs than the case with ICDs. The small vertical red lines in **Fig. 18** indicate the change in the slope and the start of the decline in the oil production due to excessive gas production. It can be observed from the figure that the well completed by AICVs has produced about twice as much oil than the well completed by ICDs at a given cumulative gas production.

Conclusions

In this study, the performance of AICV in a thin-oil-rim reservoir and its impact on reservoir recovery are evaluated. This was achieved by performing experiments and simulations. Oil production from a thin-oil-rim field can be challenging because of early gas breakthrough and high GOR. The AICVs can restrict the inflow of gas in the zones where breakthrough occurs.

The experimental work consists of one-phase and multiphase flow tests for orifice ICD and AICV using water, gas, and oil as the reservoir fluids at realistic reservoir condition. Simulations are performed using a commercial simulator. The results from experiments show that AICV restricts the gas flow significantly compared with an orifice-type ICD, specifically at higher GVF. This behavior makes this technology unique when compared with other inflow control technologies.

In the simulations, AICV/ICD tables (FCD tables) are developed based on data from the experiments. The FCD tables are used to implement the behavior of the AICV/ICD using their characteristics and the reservoir fluid properties. Hence, a workflow for developing the AICV/ICD tables in the simulator is proposed.

According to the simulation results, by completion of the well with AICVs compared with using ICDs and sand screens only, the cumulative oil production is increased by 48.7% during the first 5 years of production. Besides, AICVs reduce the cumulative gas production by 22.5% and 26.7% relative to the ICD and sand screen cases, respectively. The simulated oil production agrees with the AICV performance results from the experiments. This shows that the implementation of the workflow for generating the FCD tables in the simulator has been successful. By evaluation of the simulation results, it can be concluded that the well is producing at a beneficial GOR for a longer time for the AICV case compared with the cases with ICDs and sand screens. Keeping the GOR at a relatively low level allows the production well to stay longer at a high liquid rate without needing to choke back because of high GOR. This can be achieved by using advanced inflow control technologies such as AICVs. As it is demonstrated in this work, deploying AICVs in the most challenging light oil reservoirs with high GOR can be beneficial with respect to increased production and recovery.

Nomenclature

a_{AICD} = RCP valve/AICV strength parameter
A_{vc} = area in vena contracta
C = geometrical constant
C_d = discharge coefficient
D = diameter, m
f = friction factor, 64/Re
K_r = relative permeability
K_{rg} = relative permeability of gas phase
K_{rog} = oil relative permeability at irreducible water saturation for an oil-gas system
K_{row} = oil relative permeability for a water-oil system
K_{rw} = relative permeability of water phase
L = length, m
Q = volumetric flow rate, m^3/d
Re = Reynolds number
x = user-input parameter
y = user-input parameter
ΔP = differential pressure, bar
μ = fluid viscosity, cp
μ_{cal} = calibration viscosity, cp
μ_{mix} = mixed-fluid viscosity, cp
ρ = fluid density, kg/m^3
ρ_{cal} = calibration density, kg/m^3
ρ_{mix} = mixed-fluid density, kg/m^3

References

Aakre, H., Halvorsen, B., Werswick, B. et al. 2013. Smart Well With Autonomous Inflow Control Valve Technology. Paper presented at the SPE Middle East Oil and Gas Show and Conference, Manama, Bahrain, 10–13 March. https://doi.org/10.2118/164348-MS.

Aakre, H., Halvorsen, B., Werswick, B. et al. 2014. Autonomous Inflow Control Valve for Heavy and Extra-Heavy Oil. Paper presented at the SPE Heavy and Extra Heavy Oil Conference, Medellín, Colombia, 24–26 September. https://doi.org/10.2118/171141-MS.

Alakberi, R. S., Igein, O. F., and Aljasmi, S. A. 2023. Successful Smart Completion Deployment of Autonomous Inflow Control Valve with 13 Open Hole Segmentation Lower Completion Using a Light Workover Rig. Paper presented at the SPE/IADC Middle East Drilling Technology Conference and Exhibition, Abu Dhabi, UAE, 23–25 May. https://doi.org/10.2118/214582-MS.

Buwauqi, S., Jumah, A. A., Shabibi, A. et al. 2021. Application of Autonomous Inflow Control Valve AICV in Increasing the Field Recovery in One of the Matured Fields in the Sultanate of Oman: Case Study. Paper presented at the SPE Annual Caspian Technical Conference, Virtual, 5–7 October. https://doi.org/10.2118/207069-MS.

Canadian Legal Information Institute. 1996. *National Energy Board Act Part VI (Oil and Gas) Regulations, SOR/96-244*. https://canlii.ca/t/52hmb.

Carpenter, C. 2015. Smart Horizontal Wells for Development of Thin-Oil-Rim Reservoirs. *J Pet Technol* **67** (11): 87–89. https://doi.org/10.2118/1115-0087-JPT.

Chan, K. S., Masoudi, R., Karkooti, H. et al. 2014. Smart Horizontal Well Drilling and Completion for Effective Development of Thin Oil-Rim Reservoirs in Malaysia. Paper presented at the International Petroleum Technology Conference, Kuala Lumpur, Malaysia. https://doi.org/10.2523/IPTC-17753-MS.

Halvorsen, M., Elseth, G., and Nævdal, O. M. 2012. Increased Oil Production at Troll by Autonomous Inflow Control with RCP Valves. Paper presented at the SPE Annual Technical Conference and Exhibition, San Antonio, Texas, USA, 8–10 October. https://doi.org/10.2118/159634-MS.

Halvorsen, M., Madsen, M., Vikøren Mo, M. et al. 2016. Enhanced Oil Recovery On Troll Field By Implementing Autonomous Inflow Control Device. Paper presented at the SPE Bergen One Day Seminar, Grieghallen, Bergen, Norway, 20 April. https://doi.org/10.2118/180037-MS.

Hasan, A., Sagatun, S., and Foss, B. 2010. Well Rate Control Design for Gas Coning Problems. Paper presented at the 49th IEEE Conference on Decision and Control (CDC), Atlanta, Georgia, USA, 15–17 December. https://doi.org/10.1109/CDC.2010.5717861.

Kearns, K., Rios, F., Montero, J. et al. 2022. Autonomous Inflow Control Valves Restore Oil Production by Controlling Gas and Water Breakthrough in Acordionero Field, Colombia: A Case Study. Paper presented at the SPE Annual Technical Conference and Exhibition, Houston, Texas, USA, 3–5 October. https://doi.org/10.2118/210163-MS.

Konopczynski, M., Moradi, M., Krishnan, T. et al. 2022. Case Study: Oil Production Optimized With Autonomous Inflow Control Devices Offshore Malaysia. *J Pet Technol* **74** (09): 44–51. https://doi.org/10.2118/0922-0044-JPT.

Langaas, K., Jeurissen, E. J., and Abay, H. K. 2019. Combining Passive and Autonomous Inflow-Control Devices in a Trilateral Horizontal Well in the Alvheim Field. *SPE Prod & Oper* **34** (03): 446–460. https://doi.org/10.2118/187288-PA.

Langaas, K., Urazovskaya, O., Gueze, N. et al. 2020. Attic Oil Recovery in the Alvheim Field. Paper presented at the SPE Norway Subsurface Conference, Virtual, 2–3 November. https://doi.org/10.2118/200719-MS.

Lomeland, F. and Orec, A. 2018. Overview of the LET Family of Versatile Correlations for Flow Functions. Paper presented at the International Symposium of the Society of Core Analysts, Trondheim, Norway, 27–30 August. SCA2018-056.

Mathiesen, V., Aakre, H., Werswick, B. et al. 2011. The Autonomous RCP Valve - New Technology for Inflow Control in Horizontal Wells. Paper presented at the SPE Offshore Europe Oil and Gas Conference and Exhibition, Aberdeen, UK, 6–8 September. https://doi.org/10.2118/145737-MS.

Mjaavatten, A., Aasheim, R., Saelid, S. et al. 2006. A Model for Gas Coning and Rate-Dependent Gas/Oil Ratio in an Oil-Rim Reservoir. Paper presented at the SPE Russian Oil and Gas Technical Conference and Exhibition, Moscow, Russia, 3–6 October. https://doi.org/10.2118/102390-MS.

Mohd Ismail, I., Che Sidik, N. A., Syarani Wahi, F. et al. 2018. Increased Oil Production in Super Thin Oil Rim Using the Application of Autonomous Inflow Control Devices. Paper presented at the SPE Annual Technical Conference and Exhibition. https://doi.org/10.2118/191590-MS.

Mohd Ismail, I., Mathiesen, V., Abraham, A. et al. 2021. An Innovative Modelling Approach in Characterization of Autonomous Inflow Control Valve Performance to Maximizing Oil Recovery in Heavy Oil-SAGD Application. *SPE Thermal Well Integrity and Design Symposium*. https://doi.org/10.2118/203859-MS.

Moradi, A. and Moldestad, B. M. E. 2021. A Proposed Method for Simulation of Rate-Controlled Production Valves for Reduced Water Cut. *SPE Prod & Oper* **36** (03): 669–684. https://doi.org/10.2118/205377-PA.

Taghavi, S. and Ghaderi, A. 2021. On Uncertainty Analysis of the Rate Controlled Production (RCP) Model. Paper presented at the First SIMS EUROSIM Conference on Modelling and Simulation, SIMS EUROSIM 2021, Oulu, Finland, 21–23 September. https://doi.org/10.3384/ecp21185271.

The Norwegian Petroleum Directorate. 2019. *Zone Control for Improved Recovery and Lower Costs*. https://www.npd.no/en/facts/publications/reports/resource-report/resource-report-2019/fields/Zone-control-for-improved-recovery-and-lower-costs/.

The Norwegian Petroleum Directorate. 2021. *NPD FactPages*. https://factpages.npd.no/en/field/PageView/Producing/46437.

Timsina, R., Furuvik, N. C. I., and Moldestad, B. M. E. 2017. Modeling and Simulation of Light Oil Production Using Inflow Control Devices. Paper presented at the 58th Conference on Simulation and Modelling (SIMS 58), Reykjavik, Iceland, 25–27 September. https://doi.org/10.3384/ecp17138180.

Tusimin, F., Riyanto, L., Ahmad Tajuddin, N. et al. 2020. Enhanced Oil Production with Autonomous Inflow Control Devices in a Thin Oil Rim Reservoir Malaysia. Paper presented at the Offshore Technology Conference Asia, Kuala Lumpur, Malaysia, 2–6 November. https://doi.org/10.4043/30363-MS.

Veskimägi, V. 2013. *Gas Coning Control with a Smart Horizontal Well in a Thin Oil Rim*. PhD dissertation, Delft University of Technology, Delft, Netherlands. https://repository.tudelft.nl/islandora/object/uuid:e05799fa-2d9d-459d-afa9-fb52efb423ef?collection=education.

Appendix A—Modeling of AICV/ICD in the CMG STARS Simulator

Modeling of the AICV/ICD by using FCD tables in the CMG STARS simulators can be established as the following workflow:

1. Obtain the necessary data related to the total production rates, number of compartments, reservoir type (sandstone or carbonate), oil viscosity and density, and the desired behavior as gas shutoff and water shutoff/choking.
2. Find the available experimental data related to the case study that describe the performance of AICV for single phases of oil, gas or steam, and water. If possible, find the multiphase data of AICV too.
3. Calculate the equivalent orifice diameter by considering the same oil rate at the same pressure drop for the AICV and ICD using the following equation (Langaas et al. 2019):

$$\Delta p = \frac{1}{2}\rho \cdot \left(\frac{Q}{A \cdot C_d}\right)^2, \tag{A-1}$$

   where ΔP is the pressure drop, ρ is the fluid density, A is the flow area of the orifice, C_d is the discharging coefficient, and Q is the volumetric flow rate of fluid. By calculating A, the diameter of the orifice can be obtained. When the experimental data for an equivalent ICD is not available, Step 3 is applied.
4. Calculate the corresponding gas and water rate through ICD using Eq. A-1.
5. Generate the standard FCD table for ICDs and AICVs with optional dependencies. The optional dependency in this work is the gas mass fraction (*GFR keyword in the simulator). Total mass flow rates (*RATES_MASS keyword in the simulator) are measured for different pressure drops. One value for each combination of pressure drops and optional dependency appears immediately after the keyword *RATES_MASS. The data used in the simulation of the AICV case are presented in **Table A-1**. As it is shown in the tables for six different GFRs and four different pressure drops, the mass flow rates are measured. The first-rate Q (1) on each row must be zero and the flow rate values must be increasing monotonically. In the case of not having measurements for one data point, *EXTP may be used to either interpolate or extrapolate from adjacent values on the same table row.
6. If experimental data are not available, drive a mathematical model for the AICV using the RCP model (Mathiesen et al. 2011):

$$\Delta P_{\text{tot}} = \left(\frac{\rho_{\text{mix}}^2}{\rho_{\text{cal}}}\right) \cdot \left(\frac{\mu_{\text{cal}}}{\mu_{\text{mix}}}\right)^y \cdot a_{\text{AICD}} \cdot Q^x, \tag{A-2}$$

   where ΔP_{tot} is the pressure drop through the AICV, ρ_{cal} and ρ_{mix} are the densities of the calibration fluid and mixture fluid, μ_{cal} and μ_{mix} are the viscosities of the calibration and mixture fluid, a_{AICD} is the valve strength, and Q is the volumetric flow rate of the fluid. There are several methods to estimate the x and y, which are the parameters of the RCP valve model. These methods include but not limited to curve fitting to the experimental data, linear regression (Moradi and Moldestad 2021), and Bayesian approach (Taghavi and Ghaderi 2021).

								Definitions
*DELP		0	1000	1500	2000			**Pressure drops (kPa)
*GFR		0	0.05	0.22	0.42	0.9	1	**Gas mass fractions
*RATES_ MASS		**Q (1)	**Q (2)	**Q (3)	**Q (4)			**Rates (kg/d) across 12 valves
	1	0	96 350	111 629	135 130			
	2	0	83 520	86 000	89 000			
	3	0	39 426	42 164	*EXTP			
	4	0	14 000	14 500	15 788			
	5	0	4500	5500	6000			
	6	0	3168	3456	3744			

Table A-1—FCD table for the AICV case used in the simulations.

7. Generate the performance curves for both single- and multiphase of oil/gas and/or oil/water that represent the behavior of the AICV up to the desired differential pressure.
8. Generate the standard FCD table for ICDs and AICVs with optional dependencies as Step 5.